



OPEN UVB-induced HaCat cell damage and *Myricaria Paniculata's* molecular effects

Likuan Liu^{1,2,4}, Juan Ma^{1,4}, Wenqing Chen¹, Junyan Zhang¹, Wenming Zuo¹, Mingjin Wang¹ & Jinping Li^{1,2,3}✉

The Qinghai–Tibet Plateau, the “Roof of the World” in China, has high altitude, low pressure, thin air, little rain, long sunshine, and snow cover, causing 80–90% more Ultraviolet (UV) reflectance and greater skin UV exposure at high altitudes. *Myricaria paniculata*, a Tibetan plant growing at 2000–4500 m, has anti-inflammatory, antioxidant, and immune-boosting effects and can protect skin cells from Ultraviolet B (UVB) damage. The protective effects of *Myricaria paniculata* compounds against UVB-induced HaCat cell damage were explored. Samples were divided into normal, model, and treatment groups (seven compounds). First, the cell viability and apoptosis rates of each group were measured, along with the levels of factors such as Reactive oxygen species (ROS) and Superoxide dismutase (SOD). Network pharmacology analysis and molecular docking were subsequently performed. This study revealed that the compound enhanced cell survival, inhibited apoptosis, reduced ROS and Malondialdehyde (MDA) levels, and increased SOD activity. It also lowered the levels of Interleukin-6 (IL-6), Tumor Necrosis Factor- α (TNF- α), and Aspartate protein hydrolase 3 containing cysteine (Caspase-3). An analysis of the intersection between the 218 targets of the seven compounds found in *Myricaria paniculata* and the 1002 targets associated with skin inflammation revealed 59 common targets, with key targets including TNF and others. GO and KEGG analyses suggested the involvement of metabolic pathways. Seven core targets related to skin inflammation in *Myricaria paniculata* were identified by molecular docking. In addition, its compounds rhamnetin, rhamnocitrin, ferulic acid and kaempferol have good binding activity with TNF, PTGS2, EGFR and MMP9 targets. The Tibetan medicine *Myricaria paniculata* had a certain protective effect on UVB-induced HaCat cell damage.

Keywords *Myricaria paniculata* compounds, Network Pharmacology, HaCat cells, UVB, Molecular Docking, Antioxidant mechanism, Anti-inflammatory pathway

Abbreviations

UVB	Ultraviolet ray B
HaCat	Human Immortal Skin Keratinocytes
DMEM	Dulbecco's Modified Eagle's Medium
P/S	Penicillin/Streptomycin Solution
PBS	Phosphate buffer solution
FBS	Fetal bovine serum
MDA	Malondialdehyde
Caspase-3	Aspartate protein hydrolase 3 containing cysteine
ROS	Reactive oxygen species
SOD	Superoxide Dismutase
OD	Optical Density
CCK-8	Cell Counting Kit-8
IL-6	Interleukin-6
TNF- α	Tumor Necrosis Factor- α

¹Qinghai Provincial Key Laboratory of Medicinal Plant and Animal Resources of Qinghai–Tibet Plateau, School of Life Sciences, Qinghai Normal University, Xining 810008, Qinghai, China. ²Plateau Science and Sustainability, Qinghai Normal University, Xining 810008, Qinghai, China. ³School of Life Science, Qinghai Normal University, No. 38, Wusi West Road, Xining 810016, Qinghai Province, China. ⁴These authors contributed equally: Likuan Liu and Juan Ma. ✉email: 2008lj@163.com; 2008llk@163.com

UVB radiation can cause damages the skin significantly. ROS serve as critical mediators of the oxidative stress response and are capable of inducing degeneration of proteins and nucleic acids and lipid peroxidation, thereby causing oxidative damage to skin cells and potentially accelerating the aging process. MDA, a byproduct of lipid peroxidation, serves as an indicator of the extent of cellular damage due to free radical assault. SOD is a vital antioxidant enzyme within endogenous antioxidant systems and is responsible for decomposing free radicals generated by the body¹. Excessive UVB exposure leads to the activation of ROS within the human body^{2,3}. This oxidative stress response results in an accumulation of ROS free radicals that exceed the body's capacity for detoxification⁴. Consequently, this imbalance can cause damage to cell membranes and excessive production of MDA due to lipid peroxidation, disrupting the equilibrium between the oxidative and antioxidant systems. This disruption triggers apoptosis and cellular function loss⁵. The resulting destruction of skin cell structure and biological activity contributes to photoaging, skin tumors, and other related diseases^{6–9}. In vitro studies investigating skin damage caused by ultraviolet radiation have increasingly focused on HaCat cells, which play crucial regulatory roles in various biological processes¹⁰. Treatment with purified *Astragalus membranaceus* polysaccharide (AP) dramatically increases HaCaT cell viability and inhibits ROS generation¹¹. Liciritin can protect HaCaT cells against photoaging through mechanisms such as increased antioxidant enzyme activity and the suppression of inflammatory cytokines¹². Additionally, research has shown alterations in the expression of multiple genes during the natural aging process¹³.

Network pharmacology examines how medications, targets, and illnesses interact by combining pharmacology and systems biology^{14,15}. This method has become increasingly popular for determining the intricate ways in which medications work, particularly in the field of polypharmacology, where a single compound can interact with several targets to produce pleiotropic effects¹⁶. Network pharmacology breaks the mode of traditional drug research and development focusing on a single target, constructs a biological network by integrating multi-omics data, and studies the mechanism of drug action and the intervention effect on disease network from the system level, so as to provide new ideas and methods for drug research and development¹⁷. Currently, network pharmacology methods are increasingly used in traditional Chinese medicine research, which can link the complex chemical system of traditional Chinese medicine with the complex biological system of diseases and syndromes¹⁸. It can effectively explore the regulation mechanism of traditional Chinese medicine on disease network¹⁹.

Myricaria paniculata P. Y. Zhang et Y. J. Zhang, the tender branches and leaves of various plants in the family Tamaricaceae and the genus *Myricaria*, is a commonly used medicinal material in Tibetan medicine^{20,21}. It is primarily found in Qinghai, Xizang, Sichuan, Yunnan, Gansu, and other locations. The tender branches are flat and green, with astringent and slightly bitter tastes, which are the medicinal parts. They are mainly used for treating conditions such as “yellow water disease,” sore throat, epidemic diseases, and internal toxins²², and are known for their antifatigue and antioxidant properties, as well as their antibacterial, anti-inflammatory, analgesic, antirheumatic, and hepatoprotective effects²³. *M. paniculata* extract has a significant protective effect on CCL4-induced liver injury in mice²⁴. The chemical composition of the volatile oil from the Tibetan medicine *M. paniculata* was analyzed and identified, revealing various bioactive compounds. For example, linalool has strong antibacterial and antiviral effects; cedrol (referred to as Cedarwood alcohol) has sedative, antispasmodic, analgesic, and antiarthritic properties; and 3,5-di-tert-butyl-4-hydroxybenzaldehyde is used for the treatment of rheumatoid arthritis and osteoarthritis²⁵. In other studies, it has been found that *M. paniculata* has excellent antioxidant capacity because it scavenges free radicals, inhibits free radical production, reduces lipid peroxidation, and stimulates antioxidant enzymes²⁶. Certain phenolic compounds in *M. paniculata* have been identified as having strong antioxidant activity²⁷, and their flavonoid compounds have also been shown to have strong in vitro antioxidant capacity²¹. Recent research has unveiled that the ethanol extract of *Coriandrum sativum* L. possesses antioxidant properties, which can effectively shield the skin from photoaging induced by UVB radiation²⁸. Additionally, quercetin, a natural flavonoid renowned for its antioxidant capabilities, has been demonstrated to exert a pronounced protective influence on the skin, effectively combating oxidative damage triggered by UVB exposure²⁹. However, there is insufficient evidence to prove the protective effect of *M. paniculata* compounds on UVB-induced damage in HaCaT cells. Therefore, this study employs network pharmacology and molecular docking to investigate the inhibitory effects of *M. paniculata* compounds on UVB-induced HaCaT cell damage.

Materials and methods

Materials, reagents, and instruments

This study obtained the chemical composition of *M. paniculata* compounds through literature review³⁰. HaCat cells were obtained from Wuhan Procell Life Technology Co., Ltd., while the seven monomeric compounds were supplied by the comprehensive utilization and development research team of medicinal plant resources in Qinghai Province as part of the research group. Compounds are shown in Table 1.

DMEM high-sugar medium, penicillin-streptomycin solution (100×), 0.25% EDTA-trypsin solution (Procell Life Technology, Ltd); Cell Counting Kit-8 (Elabscience Corporation), FBS (Thermo Fisher Technologies); DMSO, PBS (Solarbio Technology Co., Ltd.); Fetal calf serum (Thermo Fisher Company); Annexin V-FITC / PI fluorescence double-dye cell apoptosis assay kit, CASP-3 enzyme-linked immunosorbent assay, TNF- α , IL-6, and SOD colorimetric assay kit (Elabscience); MDA, ROS, and TP assay kit (Nanjing Jiancheng Institute of Bioengineering).

AC2-4S1 Bioclean Workbench (ESCO Group, Singapore); HF90CO₂ incubator (Likang Biomedical Technology Holding Co., Ltd.); Infinite M200 PRO raster type multi-function microplate reader (Tecken, Switzerland); XP6 / 52 microelectron weighing term (Mettler-Toledo Group, Switzerland); IX71 inverted fluorescence microscope (Olympus, Japan); Infinite M200 PRO raster type multi-function microplate reader

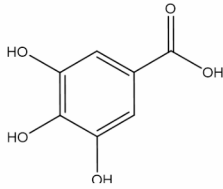
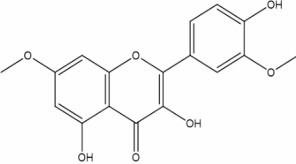
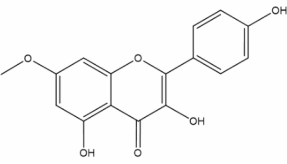
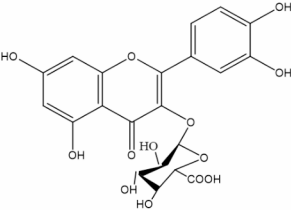
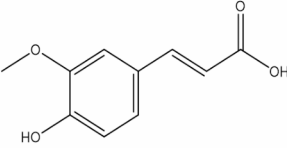
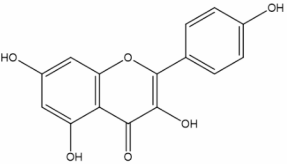
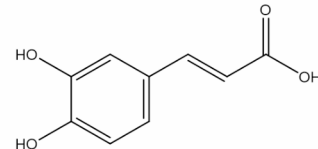
Number	Compound Name	Structural Formula
Compound 1	Gallic acid	
Compound 2	Rhamnazin	
Compound 3	Rhamnocitrin	
Compound 4	Quercetin-3-O-β-D-glucuronic acid	
Compound 5	Ferulic acid	
Compound 6	Kaempferol	
Compound 7	Caffeic acid	

Table 1. Compounds name comparison table.

(Tecken, Switzerland); Allegra X-30R high-speed frozen centrifuge (Beckman Kurt Co., Ltd.); 40 W UVB-313EL UV experimental tube; LH-125 UV irradiator (Shenzhen Guanhongrui Technology Co., Ltd.).

Cells were cultured and thawed

HaCaT cells were seeded into 25 cm² culture flasks and cultivated at 37 °C in a cell incubator saturated with 5% CO₂, containing 10% FBS and 1% P/S. When cell fusion reaches 70–90%, discard the old culture medium and wash twice with room temperature PBS buffer. Add 2–3 mL of pre-warmed 0.25% EDTA-trypsin digestion

solution at 37 °C and incubate for 8–10 min at 37 °C. When cells become round and detach, add 4–6 mL of DMEM complete medium to stop the enzymatic reaction. Transfer the mixture to a 10 mL centrifuge tube and centrifuge at 1000 r/min for 5 minutes. Discard the supernatant, add DMEM complete medium, mix well, and count the cells. Adjust the concentration to 2×10^5 cells/mL. Place the cell suspension in several culture flasks and incubate at 37 °C with 5% CO₂ until reaching 80–90% confluence. The log-phase cells were then harvested for further research.

Effects of *M. paniculata* monomeric compounds on cell viability

After the HaCat cells were expanded and allowed to acclimate to 80–90% confluence, they were digested, resulting in 2×10^5 cells per milliliter. After that, the cells were injected for 24 h at 100 µL per well in 96-well plates. The seven chemical concentration gradients were established at 3, 5 and 10 µmol/L. Furthermore, after CCK-8 was added and the cells were cultured for two hours, the cells in each chemical group were treated for 4 h, 6 h, or 8 h. The microplate reader was then warmed for 15 min, and the OD value of each well was determined at 450 nm.

UVB irradiation and cell viability assay

The distance between the cell culture plate and the UVB ultraviolet lamp is 7 cm, and the irradiation intensity measured by the ultraviolet irradiation meter is $4.0 \text{ mW} \cdot \text{cm}^{-2}$. The cells were irradiated with UVB at 5, 10, 15 and 20 min, and the upper PBS was removed. The cells were subsequently washed with PBS 1–2 times. Then, DMEM was added, and the samples were incubated at 37 °C in a 5% CO₂ incubator overnight. The next day, the OD₄₅₀ absorbance was measured after the addition of CCK-8 solution and incubation for 2 h. The data obtained were collated by Execl and plotted by OriginPro 9.1.

The effect of each group on cell survival was determined by the CCK-8 assay

The cells were randomly divided into normal, model, and compound groups, and each group had six wells. The model group was subjected to 2.4 J/cm^2 UVB irradiation. The compound group, which was exposed to 2.4 J/cm^2 UVB, was also cultured in an incubator in medium containing each compound. After treatment, CCK-8 was added to measure the absorbance, and the images were observed and analyzed under a fluorescence inverted microscope. Fluorescence intensity was measured using the AmScope software that came with the microscope.

Apoptosis of HaCat cells in each group was determined by flow cytometry

Cells were seeded in 24-well plates, and the grouping, drug administration, and UVB irradiation methods were the same as those described in the previous experiment. Afterward, the culture medium was discarded, and the cells were washed twice with PBS. Subsequently, 500 µL of $1 \times$ Annexin V Binding Buffer, 5 µL of FITC-labeled Annexin V, and 5 µL of nuclear staining solution were added sequentially, and the cells were incubated at room temperature for 15 min³¹.

Measurement of the levels of the ROS, SOD, MDA, IL-6, TNF- α , and Caspase-3 proteins in HaCat cells in each group

The cells were seeded in 6-well culture plates and sequentially grouped, subjected to UVB irradiation, and the cell ROS, SOD, and MDA levels were measured according to the instructions of the ROS, SOD, and MDA kits. The DCFH-DA fluorescence intensity was measured at an excitation wavelength of 500 nm and emission wavelength of 525 nm, and the intracellular ROS levels in each group were expressed as fluorometric values. The values of IL-6, TNF- α , and Caspase-3 were then determined according to the instructions of the IL-6, TNF- α , and Caspase-3 kits. The obtained data was organized using Excel, statistically analyzed using SPSS 25.0, and plotted using OriginPro 9.1. The inter group analysis was compared using one-way analysis of variance.

Screening of compound targets, skin inflammatory disease targets and compound–skin inflammatory target databases

The compound SMILES structures were first searched in the PubChem database (<https://pubchem.ncbi.nlm.nih.gov/>) and input to obtain the compound target sites in the Swiss Target Prediction Database (<http://www.swisstargetprediction.ch/>). From the Gene Cards Database (<https://www.genecards.org/>) and the DisGeNET Database (<https://www.disgenet.org/>), “Dermatitis” was used to screen for the retained targets of a relevance score of 1 and a score of 0.1, after which the target database of skin inflammatory disease was established³⁰. Entering these targets in VENN yields (<https://bioinfogp.cnb.csic.es/tools/venny/index.html>) common targets and a Venn diagram.

Construction of a network of skin inflammatory disease targets and potential targets

Intersecting targets were entered into the String database (https://cn.string-db.org/cgi/input?sessionId=bPfcLCJxku9q&input_page_show_search=on) to obtain the PPI network map. The relevant information is subsequently input into the Cytoscape software to further evaluate the key targets and organize the network map.

GO function, KEGG enrichment analysis, and construction of the drug–disease–component–target–pathway network

Intersection targets were fed into the DAVID Database (<https://david.ncifcrf.gov/>) for enrichment analysis and visual analysis in microbioletters (<https://www.bioinformatics.com.cn/>). Set “EASE < 0.05, Count \geq 4, FDR < 0.01, P < 0.05”. The Excel property files were constructed on the basis of the above analysis results, and drug–disease–component–target–pathway maps were constructed via Cytoscape software³².

Molecular Docking

The structural information of the receptors and ligands was downloaded from the PDB database (<https://www.rcsb.org/>) and the TCMSP database (<https://old.tcmssp-e.com/tcmssp.php>). The receptor proteins were dehydrated and dephosphorylated via PyMOL software, followed by molecular docking via AutoDockTools and AutoDock Vina software, after which the results were visualized via PyMOL software³³.

Results

Effects of different concentrations and durations of treatment on HaCat cell viability

According to the experimental results, at 4 h (Fig. 1. A), 6 h (Fig. 1. B) and 8 h (Fig. 1. C), compounds 4, 7 and 6 had the strongest effects on improving cell viability at 3 $\mu\text{mol/L}$, respectively. Therefore, 3 $\mu\text{mol/L}$ was used as the experimental concentration. The cell viability of the compounds after treatment for different durations at 3 $\mu\text{mol/L}$ is shown in (Fig. 1. D), indicating that the cell viability reached more than 100% at 6 h, so the most appropriate treatment time was 6 h.

Viability of HaCat cells after gradient UVB irradiation

Survival results of cells after gradient UVB irradiation are shown in (Fig. 1. E). The longer the irradiation time was, the lower the cell viability. At 10 min, the experimental results reached a significant level ($P < 0.05$), and the cell survival rate was 83%, so 10 min was suitable for subsequent experiments with a dose of 24 J/cm².

The viability of each group was determined via the CCK-8 assay

The results of this experiment showed a significant decrease in cell survival in the model group. The survival rate of each compound after treatment was between 61.34% and 69.52%, which was greater than that of the irradiation group, indicating that all the compound treatments improved cell viability.

Apoptosis in each group was visualized via Annexin V-FITC/PI fluorescence double staining

The staining results are shown in Fig. 2, where the model group was more abundant and stronger than the normal group was, and the two bright spots in each compound-treated group were smaller than those in the model group. Moreover, the early and late apoptotic indices of the model group were significantly greater than those of the normal group ($P < 0.01$). Compared with those of the model group, the early and late apoptotic indices of the compound treatment group were lower. The addition of available compounds reduced HaCat cell apoptosis caused by UVB.

Changes in ROS, SOD, and MDA contents and IL-6, TNF- α , and Caspase-3 contents in HaCat cells after UVB irradiation

The ROS measurement results are shown in Fig. 3, which reveals that the gray value of the model group has improved, whereas the gray value of each treatment group has significantly decreased compared with that of the model group. SOD viability decreased after UVB treatment and was significantly different from that of the normal group ($p < 0.01$); the intracellular SOD viability in the compound group increased compared with that in the model group, with SOD activity ranging between 11.84 and 26.07 U/mg prot (Fig. 4, A). Among them, the activity of SOD in the cells treated with compound 6 and compound 1 was the most significant, which was 129.29% and 109.94% higher than that in the model group. Compound 3 had the weakest increase in intracellular SOD activity (11.84 U / mgprot), which was only 4.13% higher than that of the model group (Table 2). The cellular MDA content increased after UVB irradiation, and compared with that in the normal group, the MDA content in the model group was significantly greater ($P < 0.01$), whereas the MDA content in the compound group was lower than that in the model group (Fig. 4, B). Among them, compound 6 and compound 1 treatment groups inhibited the increase of MDA content most significantly, with MDA content of 29.40 and 30.22 nmol / mgprot, which decreased by 25.55% and 23.48%, respectively (Table 3). This study revealed that *M. paniculata* compounds can reduce the contents of ROS and MDA and increase the content of SOD.

In addition, the contents of IL-6 (Fig. 4, C), TNF- α (Fig. 4, D) and Caspase-3 (Fig. 4, E) in the UVB compound group were significantly greater than those in the normal group, whereas the contents of IL-6, TNF- α and Caspase-3 in the compound group were significantly greater than those in the model group. These findings indicate that *M. paniculata* compounds can regulate and improve the inflammatory response induced by UVB.

Screening of compound targets and skin inflammation targets and acquisition of intersecting targets

The database search yielded 218 targets of *M. paniculata* and 1,002 targets related to skin inflammation. The intersection of the two genes was determined via the Venny online platform, and a total of 59 genes associated with the treatment of skin inflammation in *M. paniculata* were obtained and plotted on a Venn diagram (Fig. 5, A).

PPI network construction of *M. paniculata* compound-skin inflammation intersection targets

The PPI network was imported into the STRING database (Fig. 5, B). The key targets were further determined according to the degree value in the Cytoscape software (Fig. 5, C). The central targets are TNF (degree: 43.0), PTGS2 (degree: 31.0), EGFR (degree: 31.0), MMP9 (degree: 29.0), TLR4 (degree: 29.0), STAT3 (degree: 29.0), IL2 (degree: 28.0), MPO (degree: 21.0), and MMP2 (degree: 19.0).

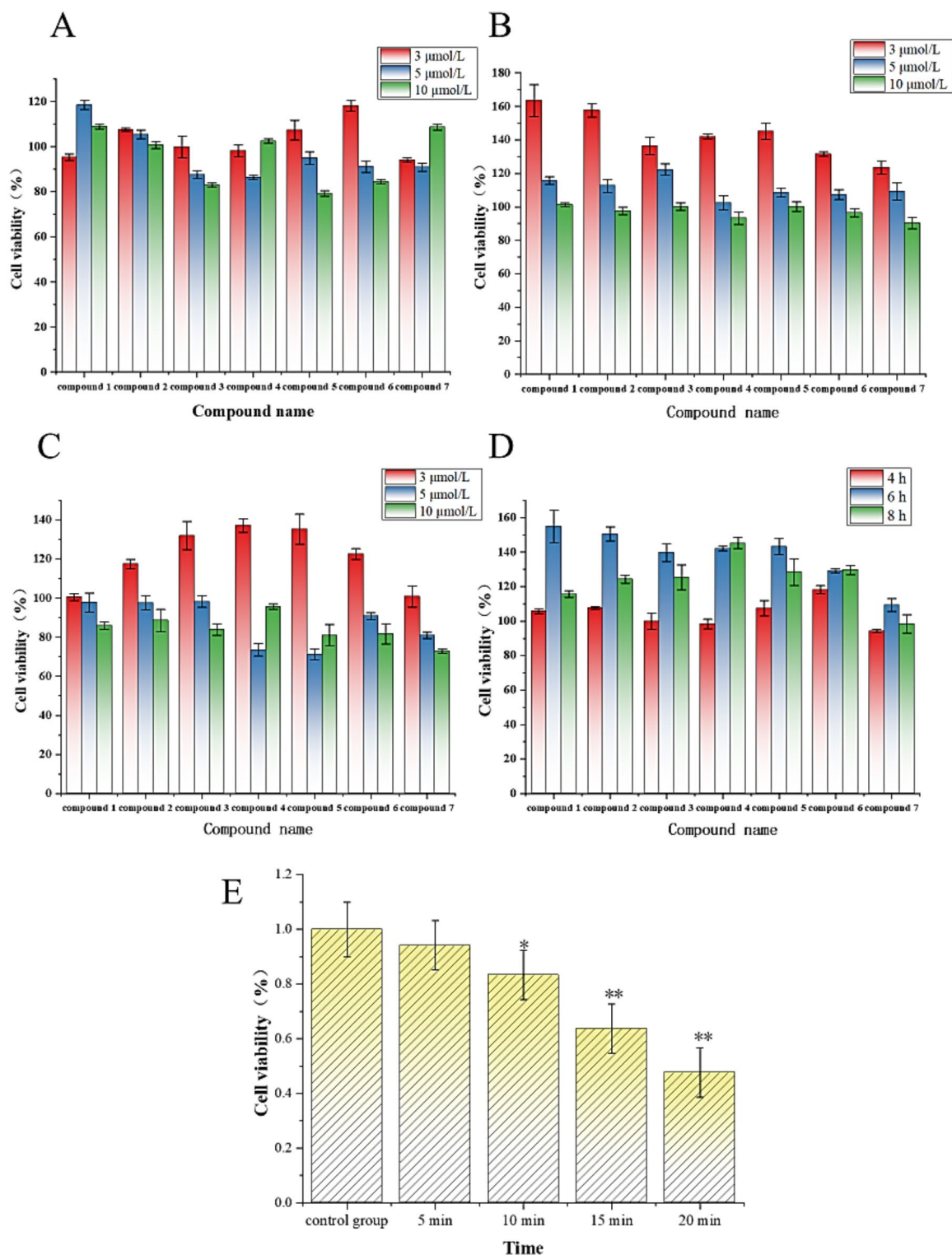


Fig. 1. Determination of cell viability values for each group (A) Cell viability at different concentrations for each compound after 4 h of treatment. (B) Cell viability at different concentrations for each compound after 6 h of treatment. (C) Cell viability at different concentrations for each compound after 8 h of treatment. (D) Cell viability for each compound at 3 μmol/L. (E) Viability for cells after irradiation with 5, 10, 15, or 20 min of UVB. *p Represents a significant difference from the controls ($p < 0.05$), and **p indicates an extremely significant difference between the controls ($p < 0.01$).

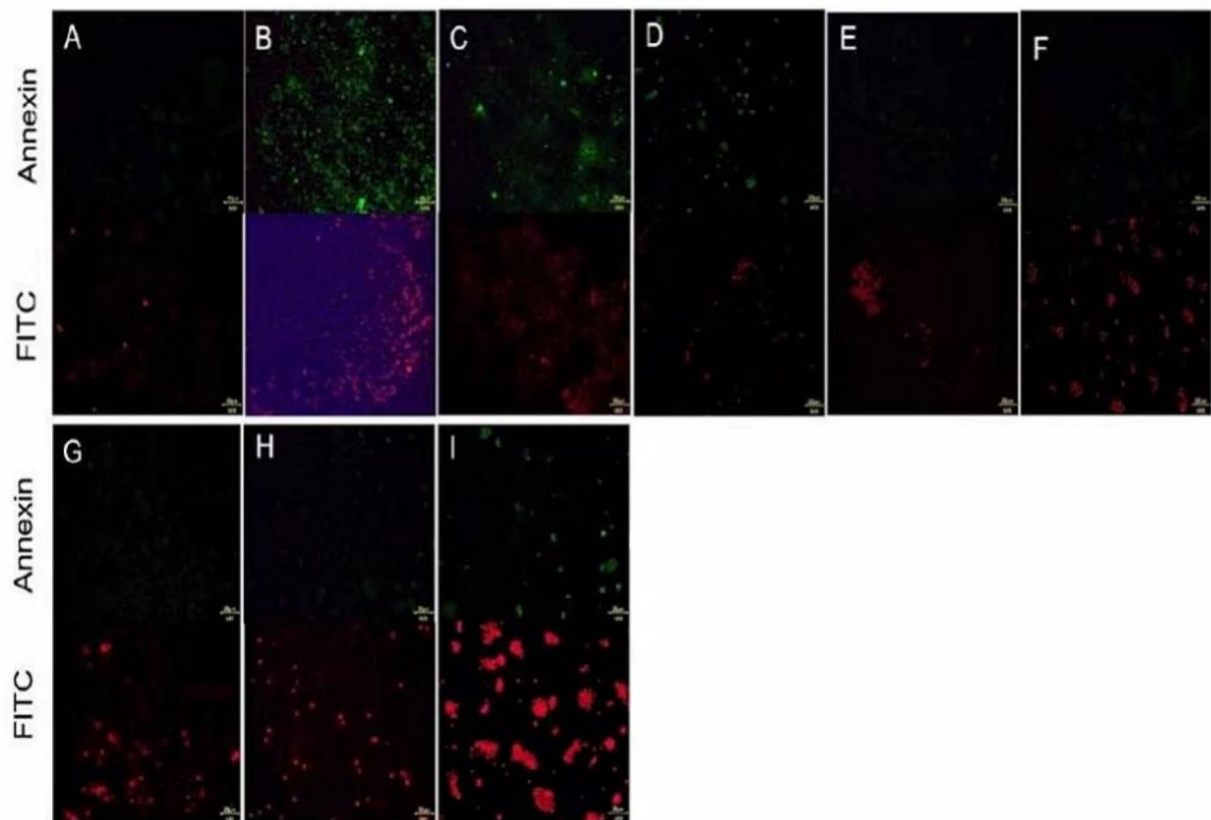


Fig. 2. Results of Annexin-FITC staining of cells in each group **A:** normal group; **B:** model group; **C:** compound 1 treatment group; **D:** compound 2 treatment group; **E:** compound 3 treatment group; **F:** compound 4 treatment group; **G:** compound 5 treatment group; **H:** compound 6 treatment group; **I:** compound 7 treatment group.

GO enrichment and KEGG pathway analysis and drug–disease–component–target–pathway network construction

The results of the GO enrichment analysis revealed that BP included 236 biological processes associated with cell aging, drug reactions, and extracellular matrix decomposition; CC included 36 processes associated with the cytoplasmic membrane, extracellular matrix, extracellular gap, etc.; and MF included 51 processes associated with zinc ion binding, endopeptidase activity, serine-type internal peptidase activity, etc. The top 15 pathways associated with logP were selected, and the groups associated with the results of the GO functional enrichment analysis were drawn, as detailed in Fig. 6. For KEGG pathway enrichment analysis, 103 pathways were selected. The targets of *M. paniculata* in skin inflammation were enriched mainly in metabolic pathways, cancer-related pathways, COVID-19-related pathways, and other signaling pathways. The top 20 pathways of the count sequence were selected for visualization, as detailed in Fig. 7. Drugs, components, diseases, and related targets and related pathways were introduced into CytoScape software to obtain drug-disease-component-target-pathways, as detailed in Fig. 8. Among them, triangles represent diseases, circles represent components, hexagons represent pathways, blue quadrangles represent drugs, and green squares represent target sites. One component in the figure corresponds to multiple targets, and one target corresponds to multiple collaterals, indicating that the compounds act through multiple pathways and multiple targets.

Molecular Docking

Four core targets, TNF, PTGS2, EGFR, and MMP9, were selected and verified by molecular docking with four *M. paniculata* compounds, Rhamnazin, rhamnocitrin, ferulic acid, and kaempferol, and the binding energies are detailed in Table 4. It is generally believed that a binding energy of less than -4.25 kcal/mol suggests that the ligand has some binding activity with the receptor, less than -5.0 kcal/mol, and strong binding activity of less than -7.0 kcal/mol³⁴. The molecular docking results revealed that the active components of the above weng cloth and the core target had better binding ability, so the predicted results were considered true and reliable, and the results with less docking energy were selected for display. The results are shown in Fig. 9.

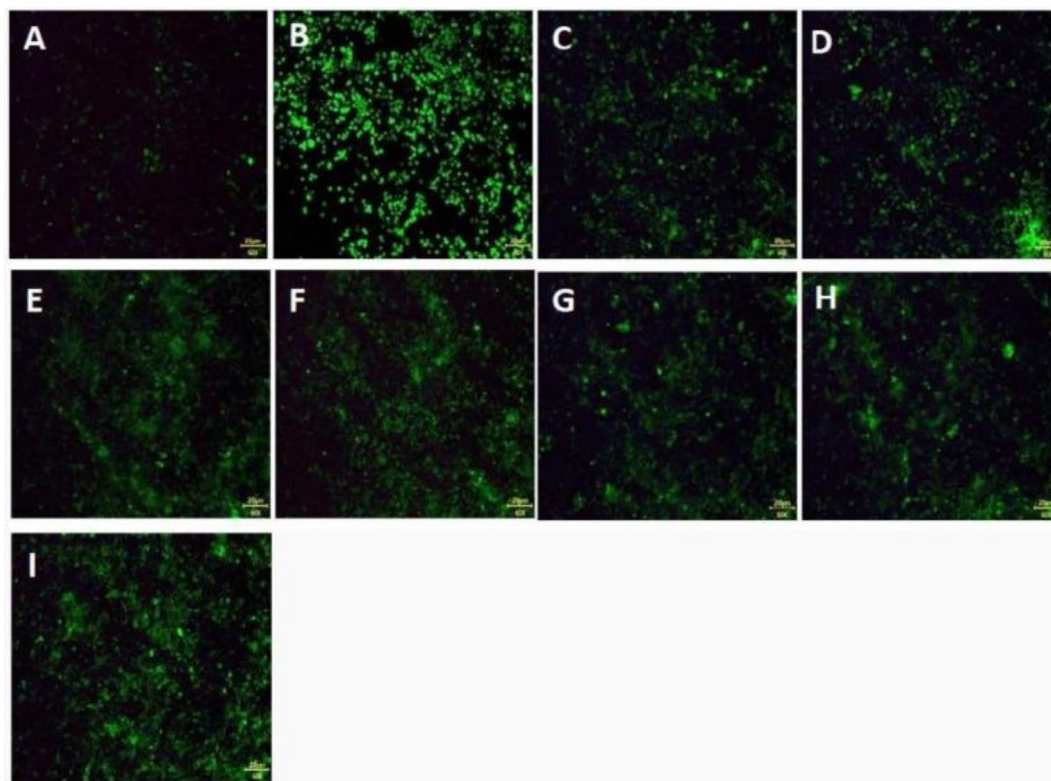


Fig. 3. Results of Annexin-FITC staining of cells in each group **A:** normal group; **B:** model group; **C:** Compound 1 treatment group; **D:** Compound 2 treatment group; **E:** Compound 3 treatment group; **F:** Compound 4 treatment group; **G:** Compound 5 treatment group; **H:** Compound 6 treatment group; **I:** Compound 7 treatment group.

Discussion

In this study, the relationship between the dosage of *M. paniculata* compounds and cell viability exhibited an “inverted U-shaped” curve, rather than a simple linear correlation. This observation indicates that an excessive dosage of the compounds does not further enhance cell viability, which may be associated with cytotoxicity at higher concentrations. This suggests that the effect of these compounds on HaCaT cells may not be direct or active. Additionally, cell survival rates were found to be positively correlated with the irradiation dose. Therefore, subsequent experiments determined the optimal compound concentration (3 $\mu\text{mol/L}$), exposure time (6 h), and irradiation dose (24 J/cm^2). Among the compounds, compound 1 had a significant impact on cell viability. Compounds 3, 4, and 6 may primarily inhibit early cell apoptosis, while compounds 2, 3, 4, and 5 may delay cell apoptosis. Compounds 3 and 4 may have minimal irritancy to the cells and exhibit stronger inhibitory effects on cell apoptosis compared to other groups. Notably, the incidence of late apoptosis was positively correlated with the concentration, whereas early apoptosis was negatively correlated. In terms of cell protection, these compounds can enhance intracellular SOD activity, reduce MDA and ROS concentrations, and decrease inflammatory factors such as IL-6 and TNF- α , as well as caspase-3 protein content, thereby resisting UVB-induced damage. Compounds that do not enhance intracellular SOD activity may primarily act on the inflammatory signaling pathways of the cells, rather than the SOD-related antioxidant signaling pathways.

Through network pharmacology methods combined with molecular docking techniques, a network analysis was conducted on the mechanisms of action of seven compounds in inhibiting skin inflammation. Key targets were docked with these compounds. The results showed that the seven core targets related to skin inflammation in *M. paniculata* include TNF, PTGS2, EGFR, MMP9, TLR4, STAT3, IL2, MPO, and MMP2. TNF- α co-cultured with endothelial cells can increase the expression of major histocompatibility complex class I antigens (MHC class I antigens) and intercellular adhesion molecule-1 (ICAM-1), promote the secretion of interleukin-1 (IL-1), granulocyte-macrophage colony-stimulating factor (GM-CSF), and interleukin-8 (IL-8), and enhance the adhesion of neutrophils to endothelial cells, thereby stimulating local inflammatory responses. Currently, TNF- α has been identified as a major regulator of inflammatory responses. *M. paniculata* may exert antagonistic effects by blocking the interaction between TNF- α and its receptors, or in some cases, acting as an agonist to stimulate reverse signal transduction, leading to apoptosis of immune cells that produce TNF- α ³⁵. However, apoptosis is a complex process regulated by multiple factors and is not dependent on a single factor. PTGS2 is the main rate-limiting enzyme for prostaglandin synthesis, which can be induced by various inflammatory mediators and cytokines, and is involved in tissue inflammation as well as cell differentiation and proliferation processes³⁶. EGFR has certain regulatory mechanisms for inflammation, mainly through the TLR family signal pathway to

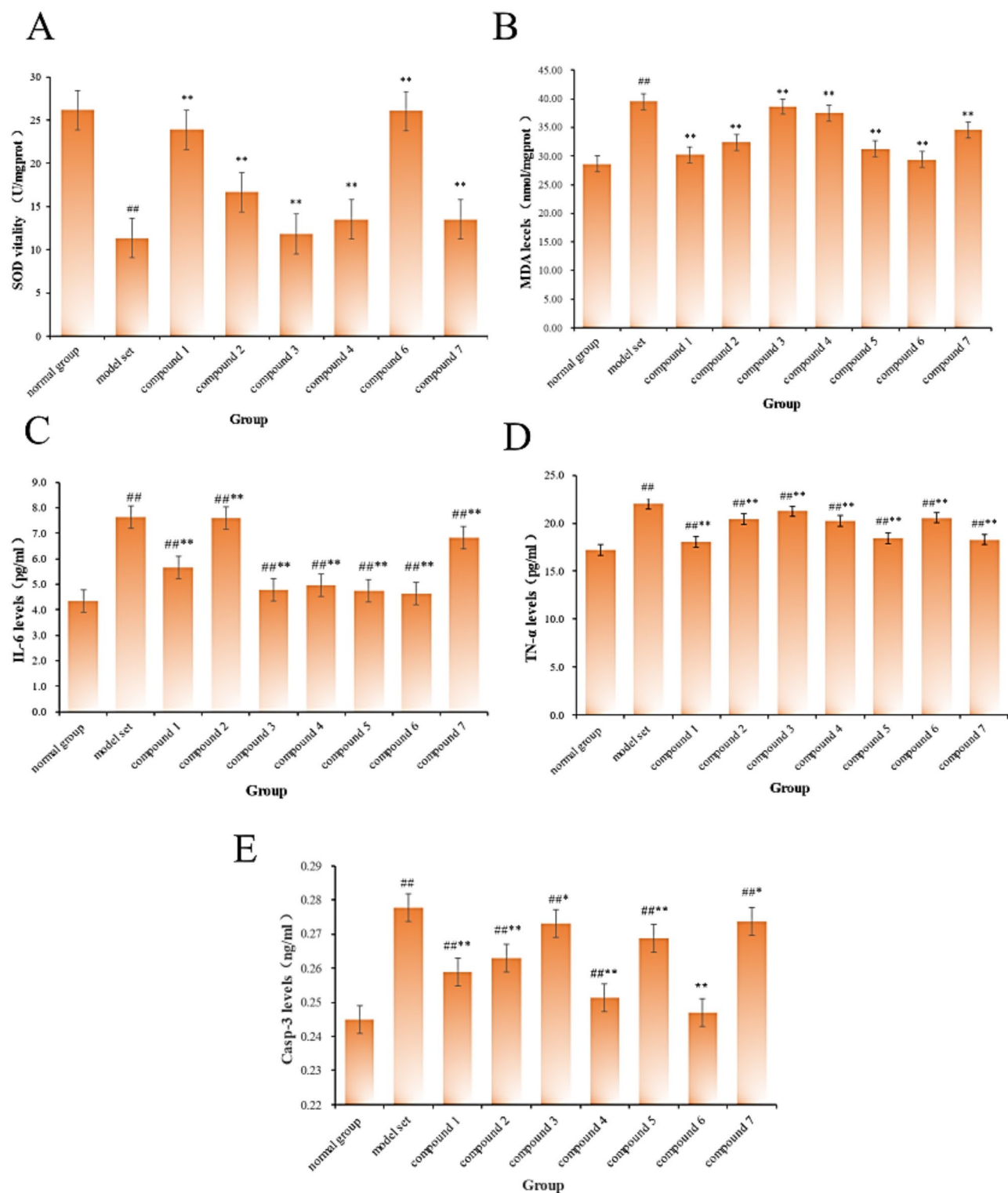


Fig. 4. Changes in measured values of HaCat cells after UVB irradiation with different compounds. **(A)** Changes in SOD activity in HaCat cells after UVB irradiation with various compounds. **(B)** Changes in the MDA content of HaCat cells after UVB irradiation with various compounds. **(C)** Effects of compounds on the content of IL-6 in HaCat cells after UVB irradiation. **(D)** Effects of compounds on the content of TNF- α in HaCat cells after UVB irradiation. **(E)** Effects of compounds on the content of Caspase-3 in HaCat cells after UVB irradiation. **p* Indicates a significant difference between the treatment and normal groups at *p* < 0.05, ***p* indicates a significant difference between the treatment and normal groups at *p* < 0.01, and ##*p* indicates a significant difference at *p* < 0.01 for the model and normal groups. The difference between each well was calculated as (survival rate of each well in each group/mean survival rate of the model group) - 1.

Group	UVB levels J/cm ²	SOD vitality U/mgprot	Difference of survival rate between each group and model group(%)
normal group	0	26.15 ± 0.018	129.99 ± 0.132
model set	24	11.37 ± 0.003##	-
compound1	24	23.87 ± 0.036**	109.94 ± 1.189
compound2	24	16.65 ± 0.101**	46.49 ± 0.796
compound3	24	11.84 ± 0.102	4.13 ± 0.803
compound4	24	13.52 ± 0.083**	18.91 ± 0.957
compound6	24	26.07 ± 0.111**	129.29 ± 0.799
compound7	24	13.50 ± 0.073**	18.73 ± 0.958

Table 2. Changes in SOD activity after UVB irradiation with various compounds. *p Indicates a significant difference between the treatment and normal groups at $p < 0.05$, **p indicates a significant difference between the treatment and normal groups at $p < 0.01$, and ##p indicates a significant difference at $p < 0.01$ for the model and normal groups. The difference between each well was calculated as (survival rate of each well in each group/mean survival rate of the model group) - 1.

Group	UVB levels J/cm ²	MDA content nmol/mgprot	Difference of survival rate between each group and model group(%)
normal group	0	28.62 ± 0.011	27.54 ± 0.023
model set	24	39.49 ± 0.011##	-
compound1	24	30.22 ± 0.016**	23.49 ± 0.01
compound2	24	32.39 ± 0.005**	17.98 ± 0.01
compound3	24	38.64 ± 0.010**	2.15 ± 0.021
compound4	24	37.50 ± 0.017**	5.04 ± 0.035
compound5	24	31.23 ± 0.010**	20.92 ± 0.021
compound6	24	29.40 ± 0.012**	25.55 ± 0.025
compound7	24	34.58 ± 0.016**	12.43 ± 0.033

Table 3. Changes in the MDA content of HaCat cells after UVB irradiation with various compounds. **p represents a significant difference between the treatment and normal groups at the $p < 0.01$ level, and ##p indicates a significant difference at the $p < 0.01$ level in the model vs. normal groups. The difference was 1 - (survival per well in each group/average survival of the model group).

induce the expression of tumor necrosis factor- α converting enzyme (TACE) or TACE-like metalloproteinases, thereby promoting the cleavage and release of transforming growth factor- β (TGF- β). TGF- α , as a ligand that binds to EGFR, activates downstream mitogen-activated protein kinase (MAPK) and phosphatidylinositol-3 kinase (PI3-K) signaling pathways after EGFR dimerization and phosphorylation, ultimately playing a role in regulating cytokine transcription. If *M. paniculata* blocks the EGFR pathway, it can reduce the expression and release of inflammatory factors, thereby alleviating skin inflammatory responses and providing a certain protective effect.

GO and KEGG analyses are instrumental in understanding the functions and pathways of core targets^{37–39}. GO pathways cover cellular senescence, drug response, and extracellular matrix degradation. Cellular senescence is closely linked to inflammation, as aging affects the immune system's ability to clear senescent cells, leading to increased inflammation. Molecular functions involve the cytoplasmic membrane, extracellular matrix, and interstitial spaces. The extracellular matrix serves as a "landing zone" for inflammatory cells, and cellular components include zinc ion binding and peptidase activity. Zinc is involved in the activity of health-related enzymes and can provide protection against ultraviolet rays and inflammation. Enhanced peptidase activity can accelerate the degradation of tachykinins to inhibit neurogenic inflammation.

KEGG pathway analysis indicates that targets involved in the treatment of skin inflammation are primarily enriched in metabolic pathways, cancer-related pathways, COVID-19-related pathways, lipids and atherosclerosis, PI3K-AKT signaling, Chagas disease, and HIF-1 signaling pathways. *M. paniculata* compounds may regulate processes such as carbohydrate metabolism, lipid metabolism, and amino acid metabolism, thereby reducing inflammatory responses. These compounds may also act on cancer-related pathways by regulating apoptosis. The regulation of COVID-19-related pathways by *M. paniculata* compounds may be associated with immune regulation and inflammation inhibition. The regulation of lipid and atherosclerosis pathways can affect the lipid composition and metabolic processes of skin cells. *M. paniculata* compounds may regulate the uptake, transport, and metabolism of cholesterol, maintaining the normal lipid structure of cell membranes and reducing oxidative stress and inflammatory responses. Activation of the PI3K-AKT signaling pathway can promote cell survival, inhibit apoptosis, and enhance the cell's tolerance to inflammatory damage, making it a key regulatory pathway for cell survival and metabolism. *M. paniculata* compounds may activate this pathway to reduce the synthesis

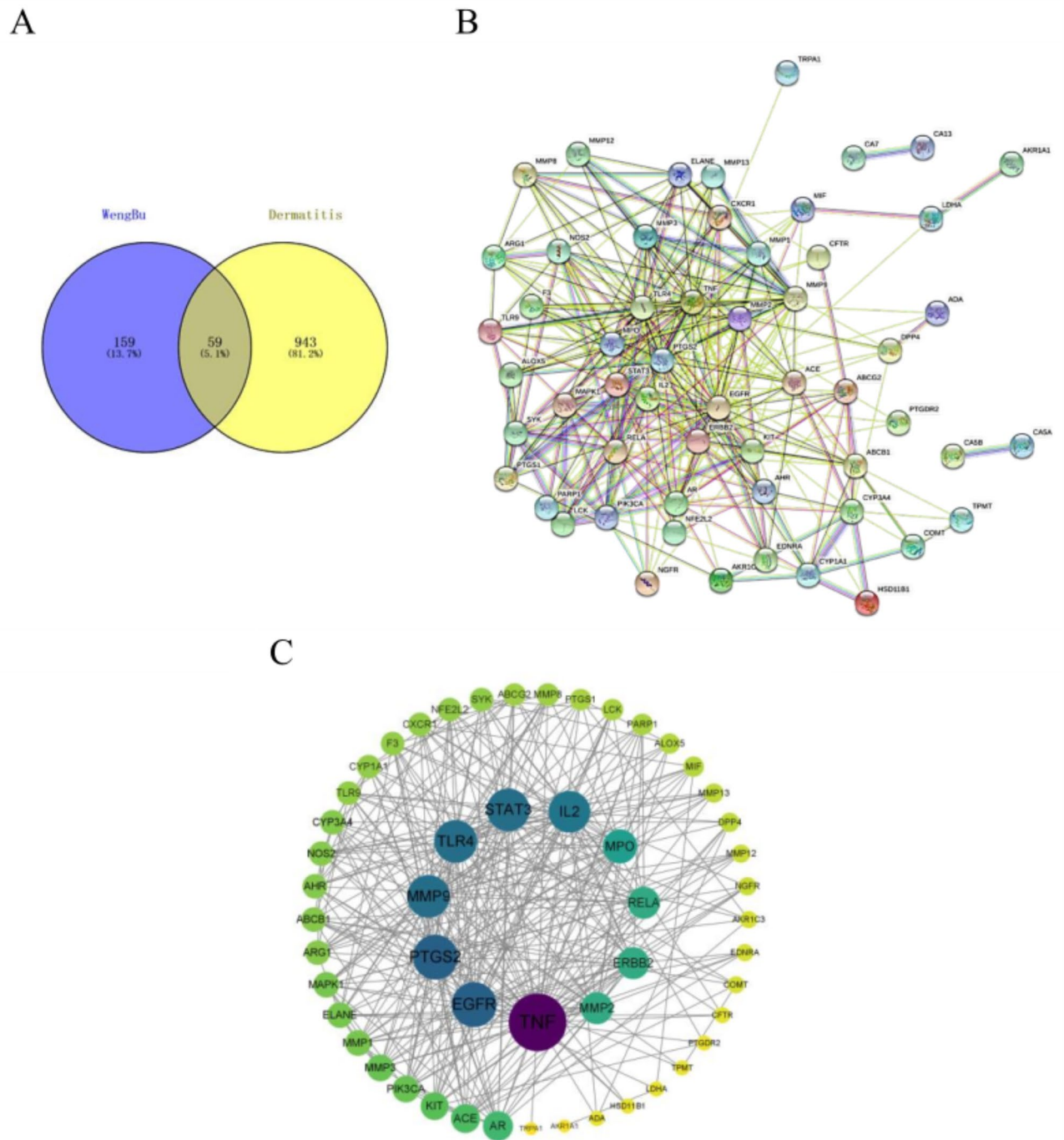


Fig. 5. Analysis of Target Comparisons, PPI Network in STRING Database and Constructed PPI Infrastructure with Cytoscape. **(A)** Venn diagram of the target comparisons. **(B)** The PPI network in the STRING database. **(C)** PPI infrastructure. The PPI network was constructed via Cytoscape. Deeper colors and larger circles indicate more critical proteins.

of inflammatory factors such as TNF- α and IL-6, thereby alleviating skin inflammatory responses. The Chagas disease pathway may involve immune regulation and stress response mechanisms within cells. The hypoxia-inducible factor-1 (HIF-1) signaling pathway: *M. paniculata* compounds may also reduce the infiltration of inflammatory cells and the release of inflammatory mediators through the HIF-1 signaling pathway, thereby reducing the degree of skin inflammation and playing an important role in the treatment of skin inflammation.

These findings indicate that *M. paniculata* compounds influence skin inflammation through multiple pathways. Molecular docking results show that *M. paniculata* compounds, such as rhamnagin, rhamnocitrin, ferulic acid, and quercetin, have good binding activity with targets such as TNF, PTGS2, EGFR, and MMP9,

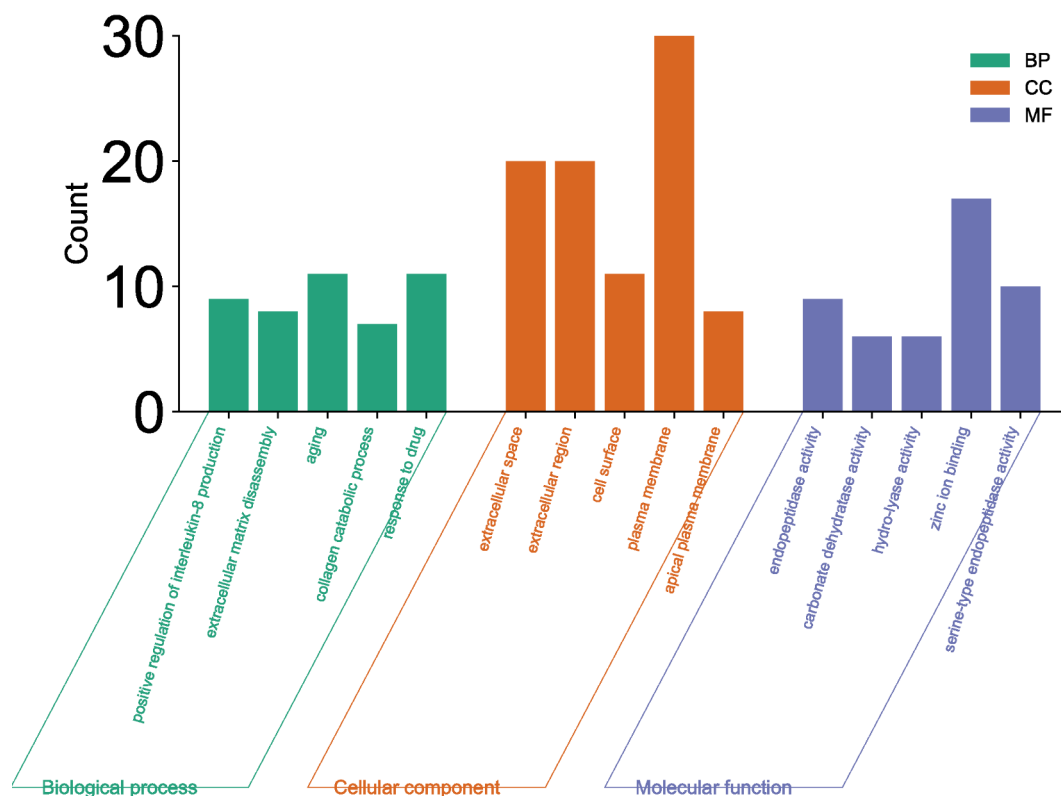


Fig. 6. GO enrichment analysis.

further confirming the therapeutic potential of *M. paniculata* as a drug. *M. paniculata* compounds have multiple potential pharmacological effects in clinical applications, but their translation and application face challenges, including the diversity of chemical components, the complexity of pharmacological effects, and the insufficiency of clinical validation.

Conclusions

In this study, we found that the seven compounds of *M. paniculata* are related to cell viability, with compound 1 having a significant impact on cell viability. Additionally, the compounds of *M. paniculata* can enhance intracellular SOD activity, reduce MDA and ROS concentrations, and decrease inflammatory factors such as IL-6 and TNF- α , as well as caspase-3 protein content, thereby resisting UVB-induced damage. The mechanisms of action were revealed through network pharmacology and molecular docking techniques, identifying seven core targets. Some of these compounds showed good binding activity with the targets. In summary, the compounds of *M. paniculata* have a certain protective effect against UVB-induced damage in HaCaT cells. Future research can use fibroblasts to evaluate the protective effects of compounds. In addition, local formulations for preclinical and clinical trials can also be developed.

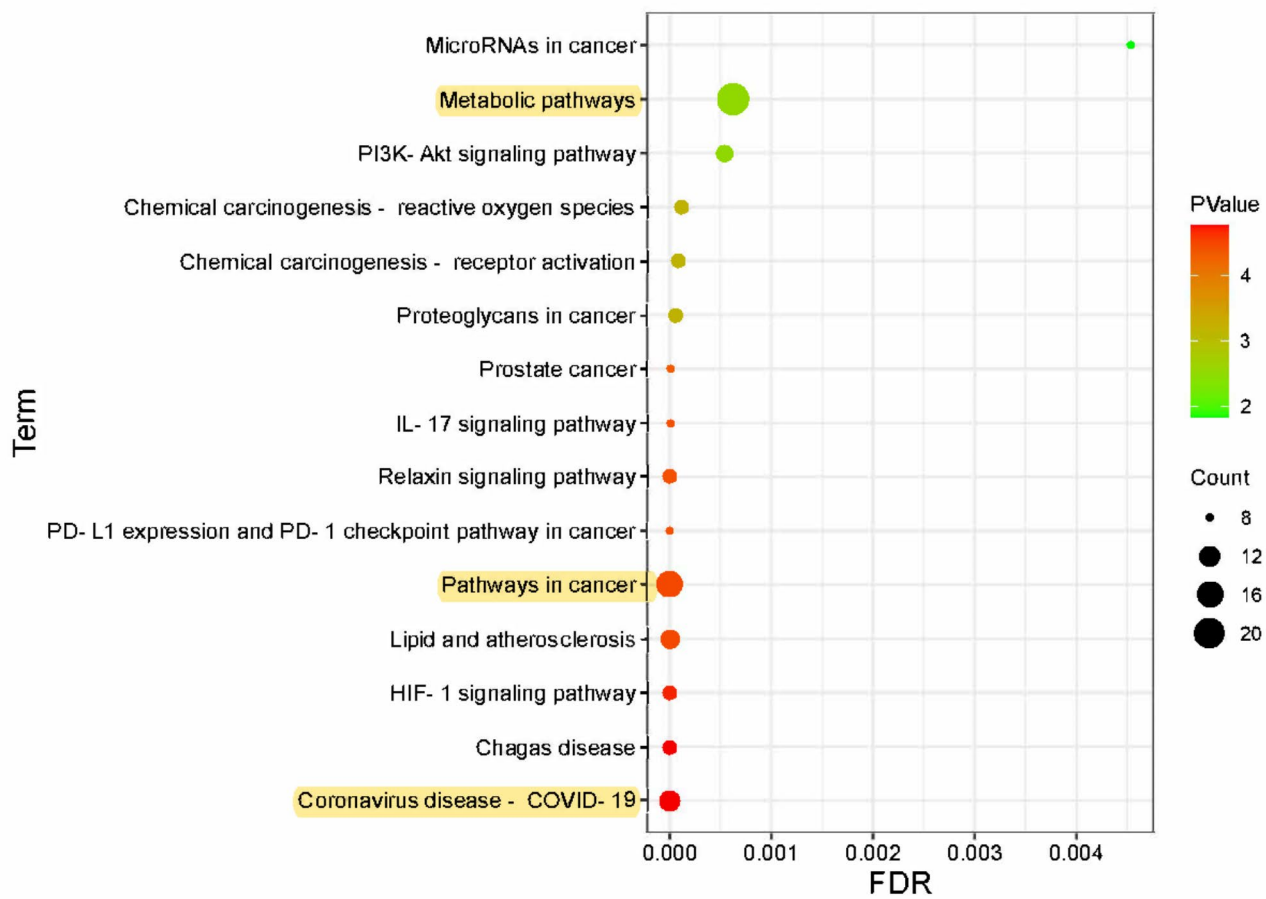


Fig. 7. KEGG analysis.

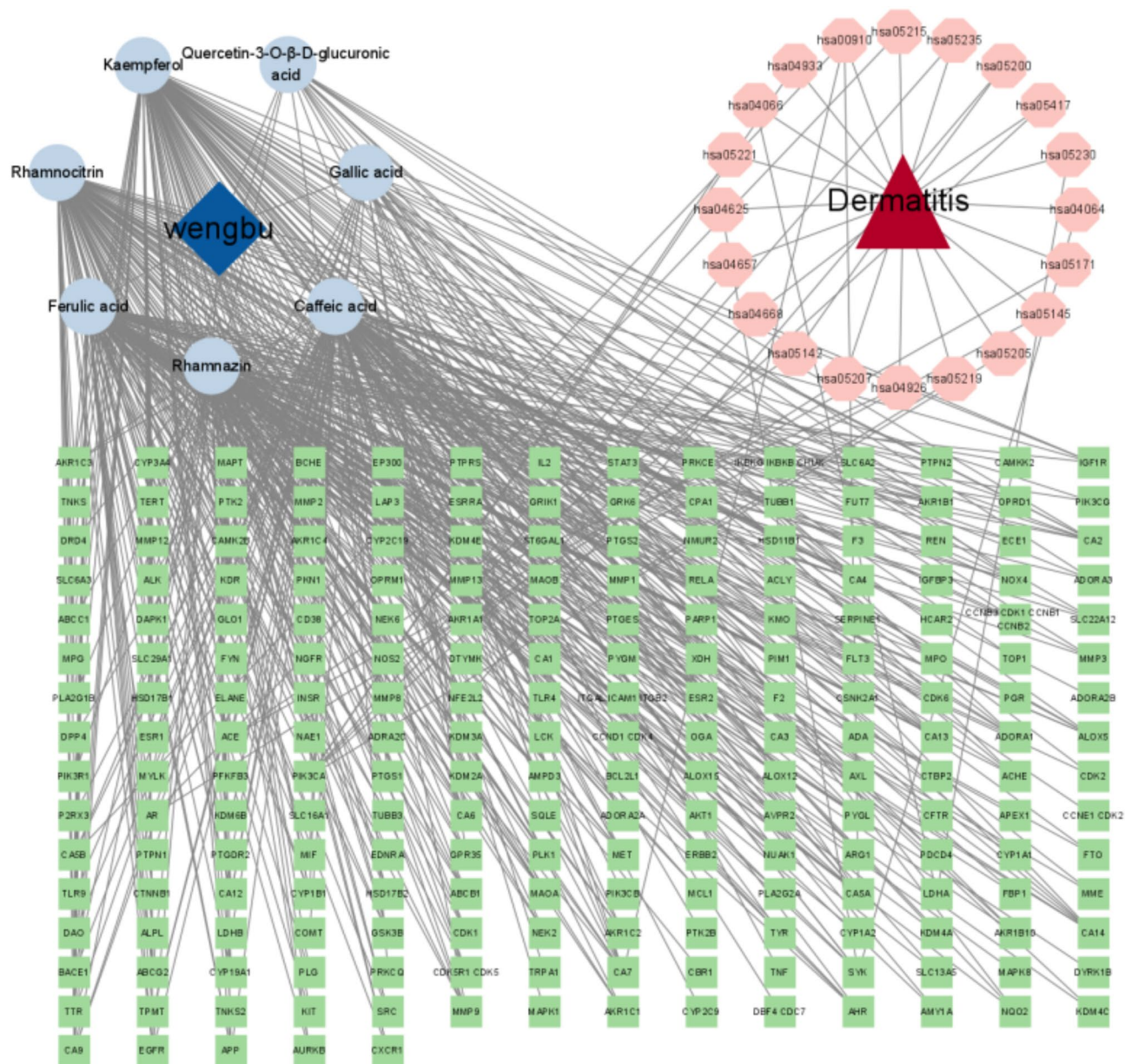


Fig. 8. Drug-disease-component-target-pathway map. Triangles represent diseases, circles represent compounds, hexagons represent pathways, blue quadrangles represent drugs, and green squares represent target sites.

compounds	TNF	PTGS2	EGFR	MMP9
Rhamnazin	-8.8 kcal/mol	-6.9 kcal/mol	-8.8 kcal/mol	-8.0 kcal/mol
Rhamnocitrin	-6.7 kcal/mol	-6.3 kcal/mol	-9.4 kcal/mol	-5.8 kcal/mol
Ferulic acid	-6.0 kcal/mol	-5.5 kcal/mol	-6.6 kcal/mol	-4.5 kcal/mol
Kaempferol	-8.6 kcal/mol	-7.3 kcal/mol	-8.4 kcal/mol	-7.5 kcal/mol

Table 4. Compounds with binding affinity to key targets.

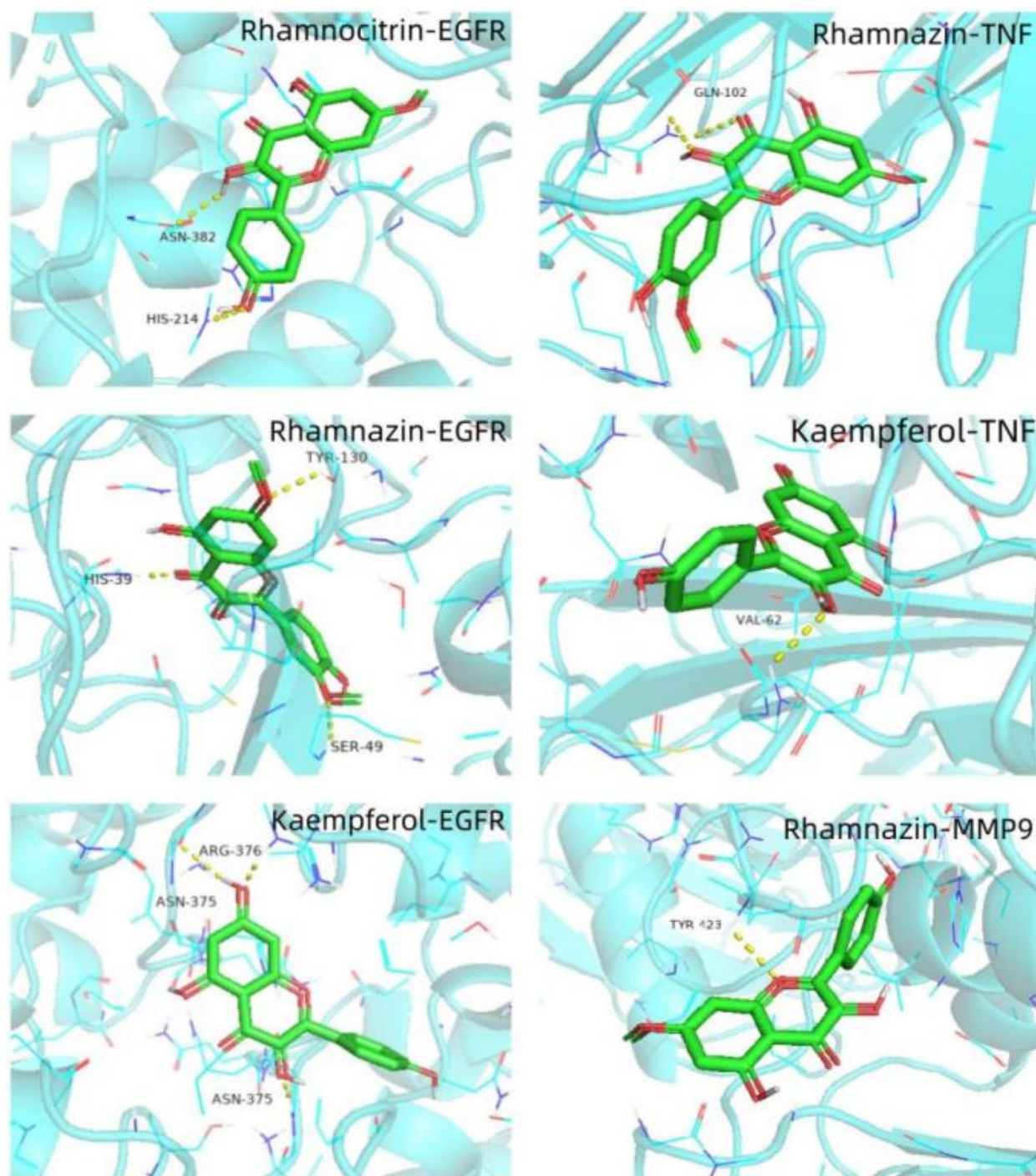


Fig. 9. Molecular docking results.

Data availability

This article provides some of the data from this study. The corresponding author may provide the dataset used in the current study upon reasonable request. The available information includes PubMed, Google Scholar, Baidu Scholar, Web of Science, SciFinder, Springer, ScienceDirect, CNKI, as well as searching for classic books on Chinese herbal medicine.

Received: 29 November 2024; Accepted: 7 March 2025

Published online: 29 March 2025

References

- Xiaoming Su, Y. et al. Anti-aging effects of schisandrin C on H₂O₂-induced HaCaT. *Med. J. Chin. People's Liberation Army*. **46** (03), 221–230 (2021).
- Kim, D. J., Iwasaki, A., Chien, A. L. & Kang, S. UVB-mediated DNA damage induces matrix metalloproteinases to promote Photoaging in an AhR- and SP1-dependent manner. *JCI Insight*. **7** (9), e156344. <https://doi.org/10.1172/jci.insight.156344> (2022).
- Gao, Q. & Zhang, L. Ultraviolet-B-induced oxidative stress and antioxidant defense system responses in ascorbate-deficient vtc1 mutants of *Arabidopsis thaliana*. *J. Plant Physiol.* **165** (2), 138–148. <https://doi.org/10.1016/j.jplph.2007.04.002> (2008).
- Si, X. Q. The Study of Protection Effects and Mechanisms of Rutin against ultraviolet-induced Skin Photodamage, Shandong University, Supervisor: Li C.Y., pp.24–26 (2011).
- Lei Xin, X. et al. Protection effect of hydroxysafflower yellow A against ultraviolet radiation injury on cultured human skin cell. *Northwest. Pharm. J.* **32** (05), 636–639 (2017).
- Liu, Y. The Preliminary Study on Astaxanthin Liposomes Anti-photodamaged Induced by UVB in Mice Skin, Southwest Medical University, Supervisor: Duan X.L., pp.6–7 (2016).
- Yum, H. W., Kim, S. H., Kang, J. X. & Surh, Y. J. Amelioration of UVB-induced oxidative stress and inflammation in fat-1 Transgenic mouse skin. *Biochem. Biophys. Res. Commun.* **502** (1), 1–8. <https://doi.org/10.1016/j.bbrc.2018.05.093> (2018).
- Xianhua Du, H. et al. Protective effect of *Panax notoginseng* saponins on skin fibroblasts damaged by H₂O₂. *Lishizhen Med. Materia Med. Res.* **22** (10), 2549–2550 (2011).
- Dandan, J. et al. Research progress of polyphenols in skin photodamage protection. *Chin. J. Aesthetic Med.* **28** (08), 158–162 (2019).
- Liu, L. S. Differential Response of NHEKs and HaCaT Cells to Hydrogen Peroxide-induced Oxidative Stress and The Defense Mechanism Study of against Oxidative Stress-induced Senescence in NHEKs, Central South University. supervisor: Xie H.F., pp.2–4.
- Li, Q. et al. Photoprotective effect of *Astragalus Membranaceus* polysaccharide on UVA-induced damage in HaCaT cells. *PLoS One*. **15** (7), e0235515. <https://doi.org/10.1371/journal.pone.0235515> (2020).
- Zhang, L. et al. Study on protective effects and mechanism of liquiritin on Photoaging HaCaT cells induced by UVB. *China Med. Herald.* **14** (36), 13–16 (2017).
- Turner, R. & Tjian, R. *Leucine Repeats and an Adjacent DNA Binding Domain Mediate the Formation of Functional cFos-cJun Heterodimers* (N.Y.), 2431689–1694 (Science (New York, 1989), 4899) <https://doi.org/10.1126/science.2494701>
- Ewes, W. A. et al. Identification of benzothiazoles bearing 1,3,4-Thiadiazole as antiproliferative hybrids targeting VEGFR-2 and BRAF kinase: design, synthesis, BIO evaluation and in Silico study. *Molecules* **29** (13), 3186. <https://doi.org/10.3390/molecules29133186> (2024).
- Abass, S. A. et al. Unraveling the Nephroprotective Potential of Papaverine against Cisplatin Toxicity through Mitigating Oxidative Stress and Inflammation: Insights from In Silico, In Vitro, and In Vivo Investigations. *Molecules*, 29(9):1927. (2024). <https://doi.org/10.3390/molecules29091927>
- Cheng, F., Kovács, I. A. & Barabási, A. L. Network-based prediction of drug combinations. *Nat. Commun.* **10** (1), 1197. <https://doi.org/10.1038/s41467-019-09186-x> (2019).
- Hopkins, A. L. Network pharmacology: the next paradigm in drug discovery. *Nat. Chem. Biol.* **4** (11), 682–690. <https://doi.org/10.1038/nchembio.118> (2008).
- Zheng, S. et al. Unveiling the Anti-Obesity potential of thunder god vine: network Pharmacology and computational insights into Celastrol-like molecules. *Int. J. Mol. Sci.* **25** (23), 12501. <https://doi.org/10.3390/ijms252312501> (2024).
- Li, S., Fan, T. P., Jia, W., Lu, A. & Zhang, W. Network Pharmacology in traditional Chinese medicine. *Evid. Based Complement. Alternat Med.* **2014**, 138460. <https://doi.org/10.1155/2014/138460> (2014).
- Northwest Institute of Plateau Biology. *TIBETAN FLORA* p. 318 (Qinghai People's Publishing House, 1991).
- Chen, H. et al. Extraction process optimization of flavonoids from *Myricaria Germanica* and its activity in vitro. *Chin. Wild Plant. Resour.* **42** (10), 57–62 (2023).
- Li, X. et al. Study on the mechanism of Tibetan medicine *Myricaria Germanica* on ulcerative colitis. *Nat. Prod. Res. Dev.* **36** (02), 206–217 (2024).
- Tang, X. et al. Chemical and Pharmacological research progress of Tibetan medicine *Myricaria Germanica*. *J. Qinghai Normal Univ. (Natural Science)*. **30** (02), 40–42 (2014).
- Bao, M. et al. Protective effects of the extract from Tibetan herb *Myricaria Germanica* P. Y. Zhang et Y. J. Zhang on mice acute hepatic injury induced by CCL₄. *J. Qinghai Normal Univ. (Natural Science)*. **26** (01), 43–46 (2010).
- Yang Zeng, R. et al. Analysis of chemical components of volatile oil from *Myricaria Germanica* by GC–MS. *Nat. Prod. Res. Dev.* **26** (05), 691–694 (2014).
- Tang, X. et al. Study on the antioxidation activity of flavonoids in *Myricaria Germanica*. *West. China J. Pharm. Sci.* **30** (01), 30–32 (2015).
- Zhang, Q. & Zeng, Y. Study on the in vitro antioxidation activity of phenolic compounds in *Myricaria Germanica*. *West. China J. Pharm. Sci.* **32** (01), 34–36 (2017).
- Hwang, E., Lee, D. G., Park, S. H., Oh, M. S. & Kim, S. Y. Coriander leaf extract exerts antioxidant activity and protects against UVB-induced Photoaging of skin by regulation of Procollagen type I and MMP-1 expression. *J. Med. Food.* **17** (9), 985–995. <https://doi.org/10.1089/jmf.2013.2999> (2014).
- Yin, Y. et al. Quercitrin protects skin from UVB-induced oxidative damage. *Toxicol. Appl. Pharmacol.* **269** (2), 89–99. <https://doi.org/10.1016/j.taap.2013.03.015> (2013).
- Zhang, J. Y. Protective effect of *Myricaria paniculata* compounds and essential oil on HaCaT cell damage caused by ultraviolet and UVB [Dissertation], Qinghai Normal University. Supervisor: Liu L.K., pp.16–19.
- Jing, W. & Deng, Q. H. Effect of phenol acid A on HaCaT cells induced by the combination of interferon γ and TRAIL and its mechanism. *Chin. Traditional Patent Med.* **43** (12), 3480–3484 (2021).
- Feifei Sun, Z. et al. Based on network Pharmacology and molecular Docking to explore the mechanism of *Sargassum fusiforme* and *Laminaria Japonica* in the treatment of thyroid nodules. *Chin. J. Hosp. Pharm.* **41** (01), 30–36 (2021).
- Haoyan Zhou, R. et al. Mechanism of Chuanxiong Rhizoma-Paeoniae Radix rubra drug pair on intervention of cerebral ischemia based on network pharmacology-molecular Docking. *Chin. J. Chin. Materia Med.* **46** (12), 3007–3015 (2021).
- Han, D. et al. Anti-depressant components and mechanism of *Rehmanniae Radix* based on UPLC-Q-Orbitrap HRMS and network Pharmacology. *Chin. J. Traditional Chin. Med.* **47** (04), 1051–1063 (2022).
- Linhui Pan. Advances in investigating the role of cytokine balance in the inflammatory response. *Med. Recapitulate* **11** (09), 775–777 (2005).
- Jianqin Liang, J. Effect and mechanism of cocompound and Q-marker prediction in rats: effect and mechanism of YAO medicine compound containing *Cissus pteroclada* on rheumatoid arthritis in rats and its Q-marker prediction. *Chin. Traditional Herb. Drugs.* **50** (19), 4705–4712 (2019).
- Kanehisa, M., Furumichi, M., Sato, Y., Matsuura, Y. & Ishiguro-Watanabe, M. KEGG: biological systems database as a model of the real world. *Nucleic Acids Res.* **53**, D672–D677. <https://doi.org/10.1093/nar/gkae909> (2025).
- Kanehisa, M. Toward Understanding the origin and evolution of cellular organisms. *Protein Sci.* **28**, 1947–1951. <https://doi.org/10.1002/pro.3715> (2019).
- Kanehisa, M. & Goto, S. KEGG: Kyoto encyclopedia of genes and genomes. *Nucleic Acids Res.* **28**, 27–30. <https://doi.org/10.1093/nar/28.1.27> (2000).

Acknowledgements

The authors would like to thank to all other authors for consulting and sorting out the relevant literature and the support of the above funds.

Author contributions

J.M. and L.L. both contributed equally to this work, and they are both listed as the first authors. The main data search and processing effort was done by L.L., W.C. and J.Z., while J.M. worked on the manuscript authoring. The concepts for the manuscript were put forth by W.Z. and M.W., who also revised the document. J.L. provided insightful feedback on the draft. The manuscript's published form was approved by all authors after they had read it.

Funding

This work was financially supported by [Applied Basic Research Project of Qinghai Province] (NO.2023-ZJ-749).

Declarations

Ethics approval and consent to participate

Ethics approval and consent to participate is not applicable for that statement.

Consent for publication

We agree to publish in your journal.

Competing interests

The authors declare no competing interests.

Additional information

Correspondence and requests for materials should be addressed to J.L.

Reprints and permissions information is available at www.nature.com/reprints.

Publisher's note Springer Nature remains neutral with regard to jurisdictional claims in published maps and institutional affiliations.

Open Access This article is licensed under a Creative Commons Attribution-NonCommercial-NoDerivatives 4.0 International License, which permits any non-commercial use, sharing, distribution and reproduction in any medium or format, as long as you give appropriate credit to the original author(s) and the source, provide a link to the Creative Commons licence, and indicate if you modified the licensed material. You do not have permission under this licence to share adapted material derived from this article or parts of it. The images or other third party material in this article are included in the article's Creative Commons licence, unless indicated otherwise in a credit line to the material. If material is not included in the article's Creative Commons licence and your intended use is not permitted by statutory regulation or exceeds the permitted use, you will need to obtain permission directly from the copyright holder. To view a copy of this licence, visit <http://creativecommons.org/licenses/by-nc-nd/4.0/>.

© The Author(s) 2025